CHAPTER FOURTEEN

PLD Protein–Protein Interactions With Signaling Molecules and Modulation by PA

J. Gomez-Cambronero*,[1], A.J. Morris†, K.M. Henkels*
*Wright State University, Boonshoft School of Medicine, Dayton, OH, United States
†The Gill Heart Institute, College of Medicine, Lexington Veterans Affairs Medical Center, University of Kentucky, Lexington, KY, United States
[1]Corresponding author: e-mail address: julian.cambronero@wright.edu

Contents

Abstract

We describe methods for studying phospholipase D (PLD) interactions with signaling proteins and modulation of these interactions by the PLD reaction product, phosphatidic acid (PA). PLD is fundamental to the physiological maintenance of cellular/intracellular membranes, protein trafficking, cytoskeletal dynamics, membrane remodeling, cell proliferation, meiotic division and sporulation. PA is an acidic phospholipid involved in the biosynthesis of many other lipids that affects the enzymatic activities of many different signaling proteins via protein–lipid interactions or as a substrate. The involvement of PLD as an effector of protein–protein interactions and downstream signaling via PA-mediated processes has led to the investigation of PA-binding domains in target protein partners. We present here data and protocols detailing the interaction between PLD2–Rac2 interaction and modulation of this interaction by PA. We describe

Methods in Enzymology, Volume 583
ISSN 0076-6879
http://dx.doi.org/10.1016/bs.mie.2016.09.042

biochemical techniques to measure interactions between PLD, PA, and the small GTPase Rac2, which are associated in the cell. We found two maxima concentrations of PA that contributed to association or dissociation of Rac2 with PLD2, as well as the PLD2 lipase and guanine nucleotide exchange factor (GEF) activities. Fluctuations in the Rac2–PLD2 protein–protein binding interaction facilitate shuttling of Rac2 and/or PLD2 within the cell dependent on local cellular PA concentration. Fluorescence resonance emission transfer stoichiometry for PLD2 and Rac2 binding yielded a 3:1 ratio of Rac2:PLD2. Detection of PA in mammalian cells with a new biosensor showed colocalization in and around the nucleus. We also described methods for quantitation of PA in biological materials by HPLC electrospray ionization tandem mass spectrometry.

ABBREVIATIONS

DOPA 1,2-dioleoyl-*sn*-glycero-3-phosphate
FRET fluorescence resonance emission transfer
GEF guanine nucleotide exchange factor
PA phosphatidic acid
PABD PA-binding domain
PBD Pak1-binding domain
PLD phospholipase D
PLD1 phospholipase D1
PLD2 phospholipase D2

1. INTRODUCTION

Phospholipase D (PLD) converts phosphatidylcholine (PC) to phosphatidic acid (PA) and choline and is important for physiological maintenance of cellular/intracellular membranes, intracellular protein trafficking, cytoskeletal dynamics, membrane remodeling and cell proliferation, and meiotic division and sporulation (Hammond et al., 1997; Powner & Wakelam, 2002; Wang, Xu, & Zheng, 1994). The initial research into PLD began with plants in the 1940s and progressed to mammals in the 1970s (Hanahan & Chaikoff, 1947a, 1947b; Saito & Kanfer, 1973). Research in the 1990s led to identification of PLD genes in plants and then in yeast and mammals in a very short period of time (Colley et al., 1997; Hammond et al., 1995; Kodaki & Yamashita, 1997; Rose, Rudge, Frohman, Morris, & Engebrecht, 1995; Wang, Dyer, & Zheng, 1993; Wang et al., 1994). Since then, PLD's involvement in lipid signaling via its main reaction product, PA, has become a topic of mounting interest to a wide variety of researchers.

PA is an acidic phospholipid involved in the biosynthesis of many other lipids that affects either directly via protein–lipid interactions or as a substrate the enzymatic activities of many different signaling proteins involved in cytoskeletal dynamics, vesicle trafficking and cell proliferation, spreading, and survival (Hermansson, Hokynar, & Somerharju, 2011; Jang, Lee, Hwang, & Ryu, 2012; Stace & Ktistakis, 2006). Interaction of protein-binding partners with PA requires a conserved polybasic amino acid domain that functions as a membrane-localization sequence, such as lipin1β, p70 S6 kinase (S6K), and aurora kinase A (AURKA) (Henkels, Mallets, Dennis, & Gomez-Cambronero, 2015; Mahankali, Henkels, Speranza, & Gomez-Cambronero, 2015; Ren et al., 2010).

PA induces production of TNFα and IL-1β in macrophages (Lee et al., 2007). IL-1β primes IL-8-activated human neutrophils for elastase release and PLD activity (Brandolini et al., 1996). IL-8 activates PLD2, while PLD-generated PA mediates IL-8 expression (Cummings et al., 2002). Stimulation with IL-8 causes a strong polarizing effect and selective accumulation of PLD2 bright caps (horseshoe formations) at the edge of the cell (Lehman et al., 2006). Additionally, the PLD–PA complex regulates fibroblast dorsal ruffle development by controlling DOCK1 cellular localization (Sanematsu et al., 2013).

Upstream signaling from tyrosine and serine/threonine kinases mediates PLD's interaction with other target proteins via direct protein–protein binding contact that influences PLD catalysis and downstream events, such as cell migration and metastatic invasion (Gomez-Cambronero, 2014). As PA is the catalytic product of the reaction of PLD with phospholipids, the involvement of PLD as an effector of protein–protein interactions and downstream signaling via PA-mediated processes has led to the investigation of PA-binding domains (PABD) on target protein partners.

2. PLD2 AND RAC2 PROTEIN–PROTEIN INTERACTION AND THE EFFECT OF PA

At least one large GTPase (dynamin) and many different small GTPases (i.e., Arf1, RalA, RhoA, Rac1, Rac2, Cdc42, Ras, and Sar1p) interact with and activate PLD via their Switch I domains, which interact with the C-terminus of PLD (Bae, Min, Fleming, & Exton, 1998; Henkels, Mahankali, & Gomez-Cambronero, 2013; Kim et al., 1998; Lee, Kim, Ghim, Suh, & Ryu, 2015; Lee et al., 2006; Pathre et al., 2003; Peng, Henkels, Mahankali, Dinauer, & Gomez-Cambronero, 2011; Peng, Henkels, Mahankali, Marchal, et al., 2011; Yamazaki et al., 1999). Likewise, PLD can regulate small GTPases via an N-terminal PA-mediated mechanism

or via the C-terminal PLD-guanine nucleotide exchange factor (GEF) activity (Chae et al., 2010; Jeon et al., 2011; Mahankali, Peng, Henkels, Dinauer, & Gomez-Cambronero, 2011).

PLD2 interacts with Rac2 via the PLD2 amino acids F107, F129, L166, R172 and L173, which is independent of PLD's lipase activity (Mahankali, Henkels, Alter, & Gomez-Cambronero, 2012). This site is also important to PLD's interaction with dynamin via R128, which further confirms a GTPase mediating a switch-on mechanism via a PLD interaction and its role as an effector (Lee et al., 2015). Once cells are stimulated, both catalytic activities of PLD2 (lipase and GEF) are upregulated. PA is quickly produced from the PLD2 lipase activity, which then positively regulates the PLD2-GEF function and activates it. GTP-bound Rac2 inhibits PLD2 lipase activity via increased PA accumulation, which upon further accumulation also interferes with PLD2-GEF binding to Rac2-GTP as substrate (Mahankali, Henkels, & Gomez-Cambronero, 2013).

3. PROTOCOL

3.1 Overview

There are numerous biochemical techniques currently being used to measure interactions between PLD, PA and the small GTPases, which range from immunoreactivity interactions as a measure of protein–protein binding to GEF activity assays in the presence of relevant protein cofactors and/or phospholipids to fluorescence resonance emission transfer (FRET) analysis via PABD on target proteins using newly developed PA sensors. Recent studies have focused on developing methods to directly measure changes in PA levels in cells and tissues, which can be used to monitor PLD activity and even determine the effectiveness of small-molecule PLD inhibitors.

3.2 *In Vivo* Rac2–PLD2 Interaction by Coimmunoprecipitation and PLD/Rac Ratio Calculations

Both PLD isoforms have many different signaling partners that bind to each other and facilitate enzymatic activities necessary for a multitude of signaling pathways required for the cell to function properly. We first suspected that the PLD2 isoform interacted with the small GTPase Rac2, as PLD and Rac were both activated with a profound effect on the kinetics of cell adhesion (Peng, Henkels, Mahankali, Dinauer, et al., 2011). We were able to determine that these two proteins are in close proximity in cells where they regulate each other via two PLD2 cdc42/Rac-interactive binding (CRIB)

domains that PLD2 uses to bind to Rac2 and modulate the biological activities of this small GTPase via other interactions with β-actin, Arp3, and β-catenin (Peng, Henkels, Mahankali, Dinauer, et al., 2011; Peng, Henkels, Mahankali, Marchal, et al., 2011; Speranza, Mahankali, & Gomez-Cambronero, 2013; Speranza, Mahankali, Henkels, & Gomez-Cambronero, 2014). We used coimmunoprecipitation (co-IP) as a tool to discern this novel interaction, whereby one protein of interest in this proposed dimer was immunoprecipitated with antibodies specific to only it, and the second protein of interest was indirectly pulled down as a result of this interaction. Additionally, the converse experimental design yielded similar protein–protein interaction results, which suggests there was no antibody epitope interference under the conditions and reagents we used.

3.2.1 Material: Rac2–PLD2 co-IP

- pcDNA3.1-HA-PLD2-WT and pRK5-myc-Rac2-WT plasmids (from Dr. Cambronero's lab) (Wright State University, Dayton, OH, USA)
- COS-7 cells for transfection (cat. # CRL-1651) (ATCC, Manassas, VA, USA)
- Transit 20/20 transfection reagent (cat. # MIR 5400) (Mirus Bio, Madison, WI, USA)
- 1,2-Dioleoyl-*sn*-glycero-3-phosphate, sodium salt (DOPA) (cat. # 840875) (Avanti Polar Lipids, Alabaster, AL, USA)
- Liposome Buffer (0.5% BSA in PBS, pH 7.2) (50 mg BSA into 10 mL of 1 × PBS, pH 7.2, make certain to check the pH)
- Rabbit α-myc and Rabbit α-HA IgG antibodies for co-IP (cat. # 2272 and 3724, respectively) (Cell Signaling, Danver, MA, USA)
- Mouse α-myc and Mouse α-HA IgG antibodies and goat antimouse HRP antibodies for western blotting (cat. # 2276, 2367, and 7076, respectively) (Cell Signaling, Danvers, MA, USA)
- Protein G Agarose FastFlow (cat. # 16–156) (EMD Millipore, Temecula, CA, USA)
- Mini-SDS-PAGE gels (cat. # 456–1094) (BioRad Laboratories, Hercules, CA, USA), Immobilon-P PVDF transfer membrane for western blotting (cat. # IPVH00010) (EMD Millipore, Temecula, CA, USA)
- SDS-PAGE Stopping Solution (1.04 g Tris base, 15 mL glycerol, 50 mg Bromophenol Blue, 9 g SDS in a final volume of 100 mL made up with good-quality water, pH adjusted to 6.7)
- Amersham ECL reagent (cat. # RPN2106) (GE Healthcare, Pittsburgh, PA, USA)
- Autoradiograph film (cat. # 100 NIF) (MidSci, St. Louis, MO, USA)

3.2.2 Protocol

1. To characterize the protein–protein interactions between the small GTPase Rac2 and PLD2, we performed co-IP experiments from COS-7 cell lysates that were mock-transfected or that overexpressed both Rac2 and PLD2 proteins via transient transfection of 2 μg pRK5-myc-Rac2-WT and/or 2 μg pcDNA3.1-HA-PLD2-WT plasmid DNAs using 5–8 μL Transit 20/20 transfection reagent per each transfection reaction.
2. Additionally, 48 h posttransfection COS-7 cells were incubated in the presence of increasing concentrations of DOPA in Liposome Buffer for 20 min to determine the effect of exogenous addition of the product of the PLD reaction (PA), according to Hatton, Lintz, Mahankali, Henkels, and Gomez-Cambronero (2015) and Mahankali, Farkaly, Bedi, Hostetler, and Gomez-Cambronero (2015). To prepare 1 m*M* DOPA stock solution, weigh out 1 mg of DOPA and add to 1.4 mL of Liposome Buffer. Sonicate twice on ice for 5 s each sonication, if bubbles form that is acceptable. Keep DOPA stock on ice to prepare final concentrations. Do not store overnight but prepare fresh daily as needed. Prepare intermediate stocks in relevant cell culture media as needed to achieve the concentration you require. Final concentrations used in our lab range from 1 n*M* to 1 μ*M* with 300 n*M* being the norm. Final volumes of your DOPA in cell culture media should be in the range of 1–2 mL added to cells in 35 mm well or 1-well of a 6-well plate. (*Note*: other phospholipids from Avanti Polar Lipids can be used in place of DOPA if you prefer, such as 1,2-dioleoyl-*sn*-glycero-3-phosphocholine (DOPC) (cat. # 850675), L-α-phosphatidylinositol (PI) (cat. # 840042), L-α-phosphatidylinositol (DOPS) (cat. # 830035), 1-oleoyl-2-hydroxy-*sn*-glycero-3-phosphate (Lyso-PA) (cat. # 857130), or phosphatidylinositol-4,5-bisphosphate (PIP_2) (cat. # 840046).
3. Following DOPA treatment, cells were either scraped from the well or trypsinized and then sedimented to acquire all of the cells from the cell culture vessel(s). Cells were lysed in 1.5-mL Eppendorf tubes using 50–150 μL Special Lysis Buffer (5 m*M* HEPES, pH 7.4, 100 μ*M* sodium orthovanadate, and 0.1 Triton X-100) + 1 mg/mL leupeptin and aprotinin protease inhibitors proteins.
4. Subsequent equal concentrations of protein from lysates (50–500 ng) were coimmunoprecipitated for 4 h at 4°C using either 1 μg Rabbit

anti-HA or 1 μg Rabbit anti-myc antibodies specific for the HA-tagged PLD2 and the myc-tagged Rac2 proteins conjugated to 20 μL Protein G agarose beads. To accomplish this step, for each reaction that you will need, first wash 20 μL Protein G agarose beads by sedimenting in 1.5 mL screw cap Eppendorf tubes at 14,000 × *g* for 1 min at 4°C. Next, aspirate the supernatant to waste using a yellow pipet tip attached to gentle vacuum suction and without disturbing the sedimented beads. Then, add 1 μg of the relevant antibody with 20 μL Protein G agarose in 100 μL Special Lysis Buffer for each reaction that you require. If you require more reactions, then just scale up accordingly. Allow the antibody–Protein G agarose complex to incubate for 1 h at 4°C with gentle rotisserie mixing, then sediment at 14,000 × *g* for 1 min at 4°C. Next, aspirate supernatant to waste as listed previously in this step.

5. Measure 1 mL of the SDS-PAGE Stopping Buffer into a 1.5-mL Eppendorf tube and add 60 μL of β-mercaptoethanol to it. Mix thoroughly. Then, resuspend pellets from Step #4 in 40 μL SDS-PAGE Loading Buffer-containing β-mercaptoethanol and heat denature at 95°C for 7 min. Then, briefly vortex and finally sediment at 14,000 × *g* for 1 min at 4°C.
6. Load only the remaining supernatants after heat-denaturing into their own individual lanes on mini-SDS-PAGE gels (i.e., 1 mm thick, 10-well 4–20% gels). Equal concentrations of protein samples (100–500 ng) were analyzed by SDS-PAGE for 1 h at 100–200 V and subsequent western blot analyses to confirm the presence of overexpressed Rac2 and PLD2 proteins in the cell lysates and level of protein–protein interaction.
7. Primary antibodies specific for Rac2 or PLD2 (or their respective tags) and then HRP-conjugated secondary antibodies were incubated sequentially with PVDFs and products visualized using ECL reagents and autoradiograph film.

As shown in Fig. 1A, Rac2 and PLD2 are both associated in the cell, as both were coimmunoprecipitated with antibodies specific for the other protein. First, HA-tagged PLD2 was immunoprecipitated with Rabbit α-HA antibodies, and when western blots were probed using Mouse α-myc antibodies, the presence of Rac2 was detected (bottom panel), as was PLD2 (top panel). Conversely, myc-tagged Rac2 was immunoprecipitated with Rabbit α-myc antibodies, and when western blots were probed with Mouse α-HA antibodies, PLD2 was detected (Fig. 1B, bottom panel),

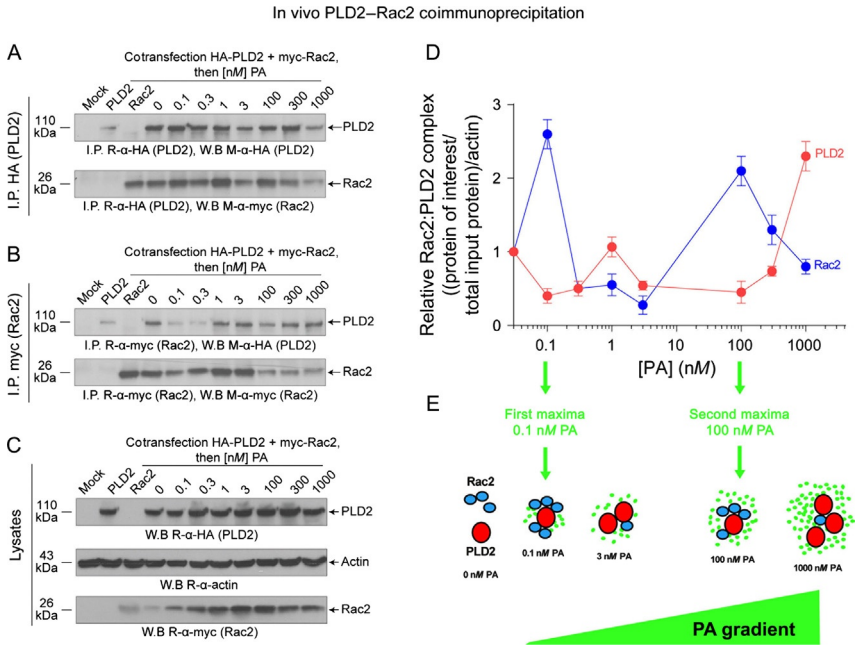

Fig. 1 Demonstration of a molecular association between Rac2 and PLD2. Coimmunoprecipitation (co-IP) of COS-7 cells overexpressing PLD2 and Rac2. Cells were transfected with HA-PLD2 and myc-Rac2 plasmids for 2 days, and PA was added directly to cells on the day of the experiment and then lysates were prepared. (A) Samples were used for co-IP with anti-HA antibodies (for PLD2), and western blots were probed with anti-myc antibodies to detect Rac2 (*bottom*) and with anti-HA antibodies to detect PLD2 (*top*). (B) Samples were used for co-IP with anti-myc antibodies (for Rac2), and western blots were probed with anti-HA antibodies to detect PLD2 (*top*) and with anti-myc antibodies to detect Rac2 (*bottom*). (C) Equal protein loading controls for both input PLD2, input Rac2, and total actin per lane prior to I.P. (D) Quantification of both Rac2 (*blue*) and PLD2 (*red*) binding from co-IP experiments shown in Fig. 1A–C in terms of protein of interest divided by total input protein of interest divided by actin. (E) Schematic representing effects of PA concentration on Rac2–PLD2-binding interaction. Note two maxima concentrations of PA that contribute to association or dissociation of Rac2 with PLD2 (0.1 and 100 n*M* PA). At maxima PA, PLD2 is optimally bound by Rac2 and not free to dissociate to function elsewhere in the cell independent of the small GTPase. Experiments were performed a total of three separate times ($n = 3$).

as was Rac2 (Fig. 1B, top panel). To confirm the presence of overexpressed/input proteins, we performed SDS-PAGE and western blot analyses of myc-Rac2 or HA-PLD2 proteins that were overexpressed in COS-7 cells and equal protein loading controls are shown in Fig. 1C, as well as actin.

PLD2 and Rac2 interacted in cells (i.e., cells ectopically transfected with PLD2 + Rac2 plasmids) (Fig. 1A and B), and in both cases, the presence of exogenous PA resulted in biphasic fluctuations in the Rac2–PLD2 protein–protein interaction (Fig. 1D). We found two maxima concentrations of PA that contributed to association or dissociation of Rac2 with PLD2 (0.1 and 100 n*M* PA). At maxima PA, PLD2 is optimally bound by Rac2 and not free to dissociate to functions elsewhere independent of the small GTPase (Fig. 1E). The strength of the Rac2–PLD2 interaction (protein–protein), which was measured using co-IP, is a function of PA availability in cells or cell media at these two maxima PA concentrations of protein–protein binding. Fluctuations in the Rac2–PLD2 protein–protein-binding interaction like this would allow shuttling of Rac2 and/or PLD2 back and forth in the cell depending on the local concentration of PA in the cell.

3.3 Rac2 Activity (GTP Loading)

There are a number of cellular signaling pathways that contribute to the transport of PLD and the product of its enzymatic reaction PA in the cell. One mechanism that could shuttle PA around and throughout the cell is that of receptor trafficking via small GTPases that occurs in cells *in vivo* as a result of growth factor-dependent stimulation. As we have shown that PA affects the binding affinity of the Rac2–PLD2 protein–protein interaction, we concentrated this next study on the effect of PA on the Rac2 GTP-binding activity, which is important for vesicular trafficking inside the cell. The tools that we used to accurately measure Rac2 activity include Pak1-binding domain (PBD) pull-down assays using Rac2 binding to Pak1 that is immunoprecipitated using Pak1 antibodies and subsequent western blot detection using Rac2 antibodies and one half of the GTP–GDP exchange reaction using PLD2 as GEF for Rac2 via the [^{35}S]GTPγS-binding reaction.

3.3.1 Material: Rac2 GTP-Binding Assays

- Purified, recombinant HA-tagged Rac2 and purified, myc-tagged PLD2 from overexpression of either the pBac-C1-6xHN-HA-Rac2-WT or the pBac-C1-6xHN-myc-PLD2-WT plasmids (Dr. Cambronero's lab) in Sf21 insect cells (Clontech)
- Rac2/cdc42 assay reagent (PAK1 PBD beads) (cat. # 14325) (EMD Millpore, Temecula, CA, USA)
- Rabbit α-HA IgG antibody to detect HA-tagged Rac2 (cat. # 3724) (Cell Signaling, Danvers, MA, USA)

- Mini-SDS-PAGE gels (cat. # 456–1094) (BioRad Laboratories, Hercules, CA, USA), Immobilon-P PVDF transfer membrane for western blotting (cat. # IPVH00010) (EMD Millipore, Temecula, CA, USA)
- SDS-PAGE Stopping Solution (1.04 g Tris base, 15 mL glycerol, 50 mg Bromophenol Blue, 9 g SDS in a final volume of 100 mL made up with good-quality water, pH adjusted to 6.7)
- Amersham ECL reagent (cat. # RPN2106) (GE Healthcare, Pittsburgh, PA, USA)
- Autoradiograph film (cat. # 100 NIF) (MidSci, St. Louis, MO, USA)
- COS-7 cells for transfection (cat. # CRL-1651) (ATCC, Manassas, VA, USA)
- Transit 20/20 transfection reagent (cat. # MIR 5400) (Mirus Bio, Madison, WI, USA)
- 1,2-Dioleoyl-*sn*-glycero-3-phosphate, sodium salt (DOPA) (cat. # 840875) (Avanti Polar Lipids, Alabaster, AL, USA)
- Liposome Buffer (0.5% BSA in PBS, pH 7.2) (50 mg BSA into 10 mL of 1 × PBS, pH 7.2, make certain to check the pH)
- RK5-myc-Rac2-WT, pcDNA3.1-HA-PLD2WT, and pcDNA3.1-HA-PLD2-K758R plasmids for overexpression in cells (Dr. Cambronero's lab)
- [^{35}S]-guanosine 5′-(γ-thio)triphosphate (cat. # NEG030X250UC) (Perkin-Elmer, Waltham, MA, USA)
- Whatman Protran BA85 nitrocellulose filter paper (cat. # 10401261), liquid scintillation vials, and Scintiverse BD liquid scintillation cocktail (cat. # SX18-4) (Fisher Scientific, Hanover Park, IL, USA)

3.3.2 Protocol

1. We first analyzed the GTP binding of purified, recombinant Rac2 in response to increasing PA *in vitro* using the PBD pull-down assay. Approximately, 19 pmol of purified Rac2 protein was incubated with increasing concentrations of DOPA (0–3 n*M*) for 20 min on ice in a 20-μL reaction.
2. Next, 5 μL of Rac2/cdc42 assay reagent (PAK-1-PBD agarose beads) was added to each sample and incubated at 4°C for 30 min in the presence of Magnesium Lysis Buffer (25 m*M* HEPES, 150 m*M* NaCl, 1% Igepal CA-630, 10 m*M* $MgCl_2$, 1 m*M* EDTA, and 2% glycerol).
3. Measure 1 mL of the SDS-PAGE Stopping Buffer into a 1.5-mL Eppendorf tube and add 60 μL of β-mercaptoethanol to it. Mix thoroughly. Then, the PA-containing, Rac2-PAK-1-PBD agarose bead

samples from Step #2 were combined with 40 μL SDS-PAGE Loading Buffer-containing β-mercaptoethanol and heat denatured at 95°C for 7 min. Then, briefly vortex and finally sediment at 14,000 × *g* for 1 min at 4°C.

4. Load only the remaining supernatants after heat-denaturing into their own individual lanes on mini-SDS-PAGE gels (i.e., 1 mm thick, 10-well 4–20% gels). Equal concentrations of protein samples (100–500 ng) were analyzed by SDS-PAGE for 1 h at 100–200 V and subsequent western blot analyses using α-HA antibodies to confirm the presence of recombinant, GTP-bound Rac2.
5. Primary antibodies specific for Rac2 (or its tag) and then HRP-conjugated secondary antibodies were sequentially incubated with PVDFs and products visualized using ECL reagents and autoradiograph film.

As shown in Fig. 2A, we found a biphasic effect of PA on Rac2 GTP loading with two maxima binding events at 0.1 and 100 n*M* PA, the effect of which is also graphically depicted in Fig. 2B. These data suggest that in the absence of PLD2, the product of the PLD reaction, PA, is sufficient to mediate a biphasic effect on Rac2 activity and that the PA lipid mediates Rac2 GTP binding.

3.3.3 Alternative Protocol

1. This pattern of PA-mediated fluctuation in Rac2 activity was also evident using an alternative method.
2. To examine if PLD2 could exchange GDP for [^{35}S]GTPγS on Rac2, 19 pmol PLD2-WT and 19 pmol Rac2 were incubated with 8 μ*M* GDP, 6 m*M* $MgCl_2$ (20 μL volume) for 10 min at room temperature.
3. GDP-bound Rac2 was added to 25 μL 100 μ*M* AMP-PNP, 1 m*M* $MgCl_2$, and 1 μ*M* [^{35}S]GTPγS in the absence or presence of PA (75 μL volume).
4. PA (0–3 n*M*) was added directly to the resulting cell lysates for 20 min at 37°C.
5. Aliquots (30 μL) were taken after the 20 min incubation period or for a different set of time (i.e., 0, 15, or 30 min) and diluted in 30 μL of STOP Buffer (10 m*M* HEPES, pH 7.4, 100 m*M* NaCl, and 5 m*M* $MgCl_2$). Samples were spotted onto Whatman BA85 nitrocellulose filters (2.53 cm^2), washed 3 × with ice-cold STOP Buffer, air-dried, and then placed into 7 mL scintillation vials containing 4–5 mL Scintiverse BD liquid scintillation cocktail.

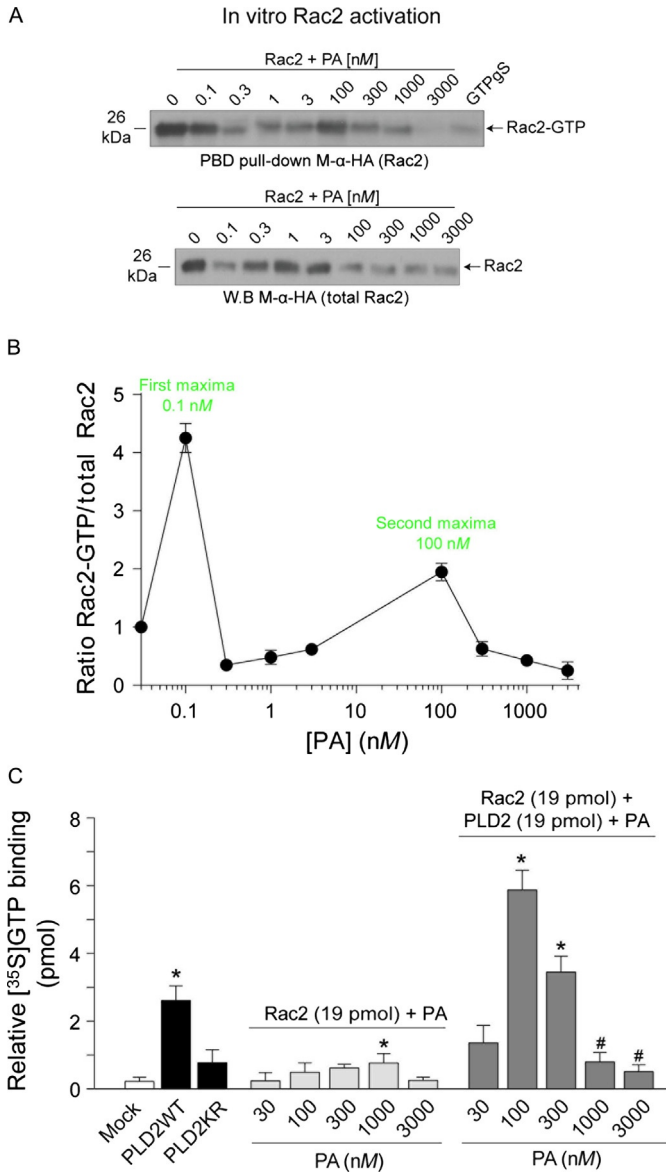

Fig. 2 Phosphatidic acid biphasically affects Rac2 GTP-binding activity. (A) *In vitro* Rac2 activation (PBD pull-down) assay using recombinant HA-Rac2 in the presence of increasing concentrations of PA (0–3 n*M*), as a readout of increased Rac2 GTPase activity due to PA. (B) Graphical representation of the ratio of Rac2-GTP divided by total Rac2 shown in (A). (C) 300 n*M* PA significantly increased PLD2-GEF-mediated Rac2 GTP loading. The (*) *symbols* denote statistically significant ($P < 0.05$) ANOVA increases between samples and controls. The (#) *symbols* denote statistically significant ($P < 0.05$) ANOVA decreases between samples and controls. Experiments were performed a total of three separate times ($n = 3$).

6. The relative amount of [^{35}S]GTPγS-bound Rac2 on the dried membranes was measured using liquid scintillation counting and expressed as picomoles bound, as in (Mahankali et al., 2011). Samples were counted in a liquid scintillation counter for 3 min intervals using an appropriate [^{35}S] protocol.
7. Purified, recombinant Rac2, PLD2-WT, and PLD2-K758R proteins were used as positive and negative controls, accordingly.

As shown in Fig. 2C, PLD2 and Rac2 interacted in cells that were ectopically transfected with PLD2 + Rac2 plasmids. Additionally, a fluctuation in Rac2 GTP loading via PLD2-GEF activity was evident in the presence of PA when PLD2 was cooverexpressed compared to Rac2 only overexpressing cells. Maximal Rac2 GTP binding occurred at 100 n*M* PA, while high concentrations of PA (>300 n*M*) resulted in inhibition of Rac2 activity. These data are consistent with that shown in Fig. 1 that used co-IP to measure the effect of PA on the Rac2–PLD2-binding interaction. PA-mediated fluctuations in the Rac2 GTP-binding activity like this could also contribute to shuttling of Rac2 via a lipid-binding mechanism, potentially as a result of PLD interaction.

3.4 FRET Stoichiometry for PLD2 and Rac2 Binding

FRET is a useful tool to investigate the spatial and molecular proximity of the proteins contained within a protein complex (Best et al., 2007; Gambin & Deniz, 2010; Kong, Polte, Alsberg, & Mooney, 2005). FRET can provide contrast between colocalized proteins of interest within a protein–protein complex better than that of conventional optical microscopy. Three criteria must be met for successful FRET: there must be a close proximity between the donor and acceptor molecules (<100 Å), the absorption spectrum of the acceptor molecule needs to have overlap with the emission spectra of the donor molecule, and the transition dipole orientations between the donor/acceptor transition need to be virtually parallel (Iqbal et al., 2008; VanBeek, Zwier, Shorb, & Krueger, 2007). Since we know that Rac2 and PLD2 can be coimmunoprecipitated and that fluorescence microscopy of stimulated leukocytes revealed an arc of Rac2 at the leading edge of pseudopodia, while PLD2 was physically posterior to the wave of Rac2 during chemotaxis (Peng, Henkels, Mahankali, Dinauer, et al., 2011; Peng, Henkels, Mahankali, Marchal, et al., 2011; Speranza et al., 2013, 2014), we hypothesized that PLD2 and its binding partner Rac2 would be suitable subjects for further FRET analysis.

3.4.1 Material: FRET Between Rac2 and PLD2

- pCerulean-C1-HA-Rac2-WT, mCit-C1-mycPLD2-WT, and mCit-N1-HA-PLD2-WT plasmids (from Dr. Cambronero's lab)
- COS-7 cells for transfection (cat. # CRL-1651) (ATCC, Manassas, VA, USA)
- FuGENE 6 transfection reagent (cat. # E2691) (Promega, Madison, WI, USA)

3.4.2 Protocol

1. To further confirm PLD2 interaction with Rac2 in the cell, the highly sensitive FRET technique was used.
2. We used mCitrine-C1-mycPLD2W-WT that contained a YFP tag as the FRET acceptor and pCerulean-C1-HA-Rac2-WT that contained a CFP tag as the FRET donor (Fig. 3A), similar to (Peng, Henkels, Mahankali, Dinauer, et al., 2011).
3. Pilot experiments were performed to determine relative levels of expression of the fluorescently tagged overexpressed Rac2 and PLD2 as determined by immunofluorescence microscopy.
4. COS-7 cells were mock-transfected or transfected with 0.5 μg CFP-Rac2 or 2 μg mCit-PLD2 plasmids in the presence of 5–8 μL Mirus Transit 20/20 transfection reagent and 48 h posttransfection, media was aspirated away from cells that were then fixed onto glass coverslips using 1 mL 4% paraformaldehyde for 10 min.
5. Cells were subsequently stained with subsequent incubations using 1:200 phalloidin-TRITC in PBS for 20 min and 1:2000 DAPI in PBS for 5 min to visualize polymerized actin and nuclei as cellular reference markers. Each of these incubations was followed by three washes with 1 mL PBS.

Resulting images shown in Fig. 3B are from merging relevant images of interest with companion TRITC- and DAPI-stained images, which indicate overexpression of FRET-tagged Rac2 and PLD2 in cells. The next logical step was to overexpress both proteins simultaneously using cotransfections prior to FRET analysis. As shown in Fig. 3C, there was considerable colocalization of both CFP-tagged Rac2 + mCit-tagged PLD2 to the nucleus and vesicular locations, which suggests potential protein–protein interaction between PLD2 and Rac2. Vesicles could be used for both the delivery and retrieval of PLD2 to the plasma membrane during agonist stimulation once the small GTPase Rac2 has been delivered to the plasma membrane.

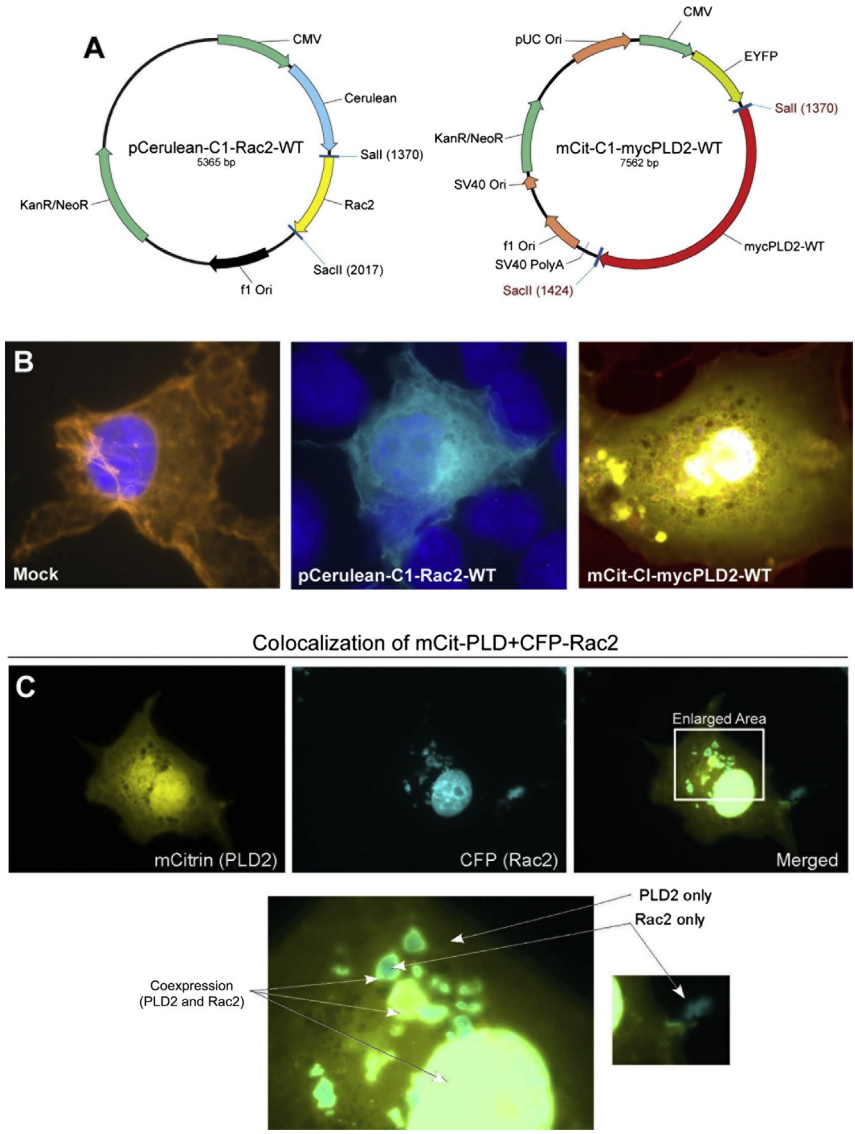

Fig. 3 Overexpressed fluorescently tagged PLD2 and Rac2 colocalize in cells. (A) Vector maps of fluorescently tagged Rac2 and PLD2 plasmids used for FRET. (B) Immunofluorescence microscopy of mock-treated or overexpressed CFP-Rac2 and mCit-PLD2 proteins in COS-7 cells, respectively. Polymerized β-actin was visualized using phalloidin-TRITC staining for mock- and PLD2-transfected cells only, and nuclei were stained in all samples with DAPI. Resulting images shown are from merging relevant image of interest with companion TRITC- and/or DAPI-stained images. (C) Immunofluorescence microscopy of COS-7 cotransfected with CFP-tagged Rac2 + mCit-tagged PLD2, as either independent images or merged image. *Lower panels*, enlarged area of merged image. Shown in this figure are images representative of $n = 3$ independent experiments with visualization of five similar fields from each condition.

To establish the existence of FRET between PLD2 + Rac2, COS-7 cells were cotransfected with equimolar concentrations of PLD2-mCitrine and Rac2-mCFP using FuGENE 6 reagent for 48 h (the cells were serum-starved for the last 16 h) so that, therefore, neither protein was in excess following overexpression. When ready for microscopy, cells were left unstimulated. Fluorescence microscopy was performed with appropriate excitation and emission filter sets (Chroma Corporation) for CFP, YFP, and FRET (CFP excitation and YFP emission). Images were collected on a 14-bit Cascade HQII digital camera and were processed as described in Hoppe et al. to determine the FRET stoichiometry of the interaction between PLD2 and Rac2 (Hoppe, Christensen, & Swanson, 2002).

Fluorescence imaging showed FRET microscopy localized to the nucleus in the absence of any stimulation in the following images shown in Fig. 4A: I_a (PLD2-mCitrine), I_d (Rac2-mCFP), and I_f (FRET) images, as labeled on the left. Calculated FRET images are E_a, E_d, and R_m, as labeled on the right. The mean average FRET efficiency was predominantly in the

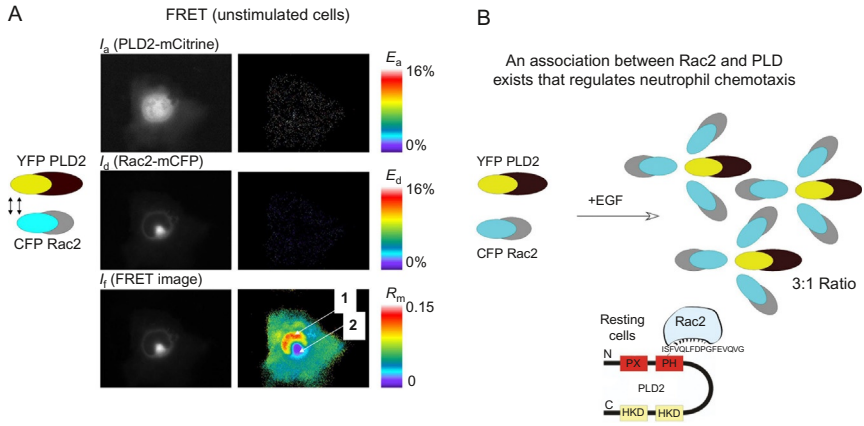

Fig. 4 Demonstration of FRET between fluorescent-tagged PLD2 and Rac2. (A) COS-7 cells were transfected with mCit-PLD2 (FRET acceptor) and CFP-Rac2 (FRET donor) for 48 h. When ready for FRET, cells were left unstimulated. Microscopic images shown FRET in the nucleus: I_a (mCit-PLD2), I_d (CFP-Rac2), and I_f (FRET) images. *Color panels* on right show predicted FRET images: E_a, E_d, and R_m, magnitude of E_a, E_d, or the ratio of the acceptor to the donor molecules (R_m), respectively. (B) Model of PLD2–Rac2 stoichiometry during neutrophil chemotaxis. Rac2 has a dual effect on PLD2 that controls the onset and termination of leukocyte chemotaxis, which is mediated by the accumulation of excess Rac2 GTPase compared to PLD2 in the cells.

nucleus (*E*avg) as determined using Metamorph and Matlab software and which reached a maximum of 0.15. For comparison, the linked CFP-Citrine positive control used for calibration of the microscope yielded an *E*avg of 0.37. Control experiments cooverexpressing mCitrine-PLD2 and free-CFP showed no FRET. The existence of FRET using mCit-PLD2 and CFP-Rac2 overexpression under equimolar conditions shows that PLD2 and Rac2 are in close enough proximity in the cell's nucleus to form a stable heterodimeric complex (<7 nm distance).

Data shown here and in other studies suggest that cytoplasmic localization of Rac2 + PLD2 to vesicles is both dependent and independent of cell stimulation. Rac2 interacts with and binds to PA-containing vesicles in neutrophil cytosol, which suggests that PLD2 mediates this process (Faugaret, Chouinard, Harbour, El azreq, & Bourgoin, 2010). Further, Rac2 has a dual effect on PLD2 such that a positive-feedback loop controls the onset of leukocyte chemotaxis, while Rac2-led PLD2 inhibition mediates the termination of leukocyte chemotaxis, which is mediated by the accumulation of excess Rac2 GTPase compared to PLD2 in the cells (Fig. 4B; Peng, Henkels, Mahankali, Marchal, et al., 2011).

3.5 Detection of PA in the Cells With a Biosensor

The use of a biosensor as a tool to detect cellular PA has been extensively characterized from sporulation-specific protein 20 (Spo20p), which is a yeast protein required for the fusion of exocytic vesicles with the plasma membrane during yeast sporulation through its interactions with the soluble *N*-ethylmaleimide sensitive-factor attachment protein receptor (SNARE) complex (Nakanishi, de los Santos, & Neiman, 2004; Zeniou-Meyer et al., 2007; Zhang et al., 2014). Spo20p is a dual function protein that contains both an inhibitory region that sequesters the protein in the nucleus and a positive regulatory region that binds to phospholipids in the cell membrane (Nakanishi et al., 2004). This positive regulatory region comprises a 40-amino acid region (51–91) containing an amphipathic helix with hydrophobic and positive charges that binds to cell membrane phospholipids and preferentially to PA, which has been termed the PABD. Wild type and mutant enhanced green fluorescent protein (EGFP)-tagged Spo20PABD plasmids have been used to visualize PA localization in mammalian cells in previous studies by many different labs. Some of the difficulties other researchers have encountered while using this EGFP-tagged PABD sensor

include lack of response using moderate stimulation or ligands specific to membrane-bound receptors. EGFP-tagged proteins have been widely utilized to monitor cellular processes, which is fully dependent on EGFP being a completely passive reporter protein.

Evidence suggests that two populations of EGFP have the potential to exist in cells, one being cytosolic and monomeric and the other being secretory, nuclear, and oligomeric (Chen, Muller, Ruan, & Gratton, 2002; Jain, Joyce, Molinete, Halban, & Gorr, 2001). The use of EGFP-tagged vectors has evolved to the next generation of monomeric pAcGFP plasmids to circumvent the issue of EGFP oligomerization (Gurskaya et al., 2003; Matz et al., 1999). Therefore, the Spo20 PABD sequence comprising amino acids 51–91 (MDNCSGSRRRDRLHVKLKSLRNKIHKQLHP NCRFDDATKTSDDKC) was subcloned into the pAcGFP-C1 and pAcGFP-N1 vectors using *Bgl*II and *Eco*RI or *Xho*I and *Bam*HI, respectively (Mutagenex, Suwanee, GA, USA) (Fig. 5A and B), which we used as our biosensor for cellular PA localization following transient transfections (Fig. 5C).

3.5.1 Material: PLD and the PA Sensor Colocalize in Cells

- pAcGFP-C1-PABD-WT, pcDNA3.1-mycPLD2-WT, and pcDNA3.1-mycPLD2-K758R *plasmids* (Cambronero's lab)
- 5-Fluoro-2-indolyl des-chlorohalopemide (FIPI) (cat. # 13563) (Cayman Chemical, Ann Arbor, MI, USA)
- Rabbit α-PLD2 IgG (H-133) antibody and goat antirabbit FITC IgG antibody (cat. # sc-25513 and sc-2012, respectively) (Santa Cruz Biotechnology, Santa Cruz, CA, USA)
- 4′,6-Diamidino-2-phenylindole (DAPI) (cat. # D1306) (Invitrogen, Carlsbad, CA, USA)
- Human epidermal growth factor (EGF) (cat. # 300-110P) (Gemini Bio-Products, West Sacramento, CA, USA)
- COS-7 cells (cat. # CRL-1651) (ATCC, Manassas, VA, USA)
- Transit 20/20 transfection reagent (cat. # MIR 5400) (Mirus Bio, Madison, WI, USA)
- Starvation Media (DMEM + 0.1% BSA, sterile filtered)
- Glass coverslips and microscope slides
- Vectashield immunofluorescence mounting media (cat. # H-1000) (Vector Labs, Burlingame, CA, USA)

We next studied intracellular localization of endogenous and overexpressed PLD2 compared to that of the overexpressed PA sensor. Our rationale is that

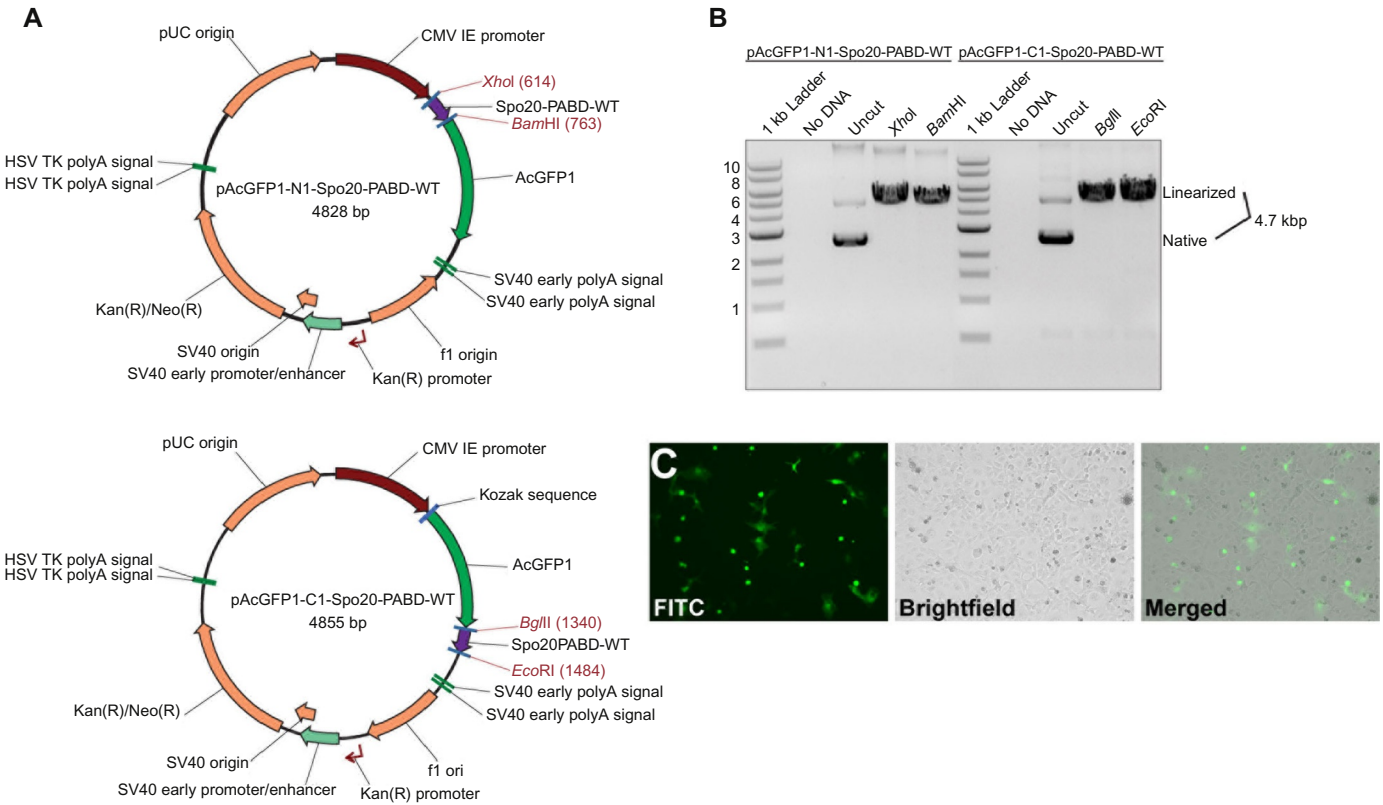

Fig. 5 Generation of a new PABD sensor into a monomeric GFP vector. (A) Vector maps of N-terminal and C-terminal Spo20-PABD AcGFP-tagged plasmids used for colocalization with PLD protein in cells. (B) Restriction enzyme digestion of cloning scheme: Spo20 PABD was cloned into pAcGFP-N1 vector using *Xho*I and *Bam*HI, while *Bgl*II and *Eco*RI were used for cloning into the pAcGFP-C1 vector. (C) Immunofluorescent and brightfield microscopic images (20 ×), indicating a positive result for overexpression of pAcGFP-C1-Spo20-PABD-WT into COS-7 cells 48 h posttransfection of 1 μg of plasmid DNA.

if the PABD of the PA sensor actually binds to PA then we would expect a similar localization pattern as that of PLD2. For this to occur, we confirmed the cellular localization pattern of both PLD2 and the PA sensor using mammalian cells.

3.5.2 Protocol

1. COS-7 cells were plated onto glass coverslips contained in 35 mm wells or 6-well plates and then once adhered were transfected with 2 μg of the GFP-tagged Spo20-PABD sensor or the myc-tagged PLD2 (either WT or lipase-inactive K758R) plasmids using 5–8 μL Transit 20/20 transfection reagent per each transfection reaction.
2. Forty-eight hour posttransfection cells were serum-starved for 2 h using 1 mL Starvation Media per each well. At this point, cells were next untreated or treated with the addition of a final concentration of 300 n*M* FIPI added directly to the 1 mL Starvation Media already on the cells for 20 min and then unstimulated or stimulated with a final concentration of 10 n*M* human EGF for 15 additional minutes. (*Note*: to prepare the FIPI and EGF stock solutions, initially prepare each stock solution so that it is ~1000 × more concentrated than the final required concentration. Therefore, prepare 300 μ*M* FIPI and a 10 μ*M* EGF stock solutions. Also, check the manufacturer's recommendations for initial solubilization for each compound. Once correctly solubilized, each compound can then be diluted accordingly into the correct/relevant buffer.)
3. Cells were fixed with 1 mL of 4% paraformaldehyde, permeabilized with 0.1% Triton X-100 in PBS, pH 7.4, blocked for 4 h in blocking buffer (5% BSA in TBS-T), stained with α-PLD2-TRITC antibodies in blocking buffer (5% BSA in TBS-T) for 1 h to overnight to visualize either overexpressed PLD2 or endogenous PLD2, washed 3 × with 1 mL PBS for 5 min each wash and then with 1 mL of 1:2000 DAPI in PBS for 5 min to visualize nuclei, and then lastly followed by another set of washes 3 × with 1 mL PBS for 5 min each wash. Coverslips were washed once briefly with water and then allowed to air-dry. Once dried, coverslips are then mounted onto glass microscope slides using Vectashield mounting media. Allow slides to set overnight and then paint the edge of the coverslip with clear nail polish to seal the slides. Once the nail polish is completely dry, it is safe to proceed to microscopy.

4. The PA sensor was visualized using its GFP tag and therefore a FITC filter. PLD2 was visualized using the TRITC filter, while DAPI was visualized using the UV filter.
5. Merged images of overlaid FITC and DAPI images or TRITC and DAPI images are shown.

Immunofluorescence microscopic images of COS-7 cells indicate that overexpression of either the Spo20-derived PABD sensor or PLD2-WT resulted in nuclear/perinuclear accumulation of the PA sensor and PLD2-WT in the absence of EGF stimulation (control) (Fig. 6A, top panels), which was abrogated following EGF stimulation for 7–15 min (Fig. 6A, bottom panels). Additionally, preincubation of cells with either a PLD-specific inhibitor (300 n*M* FIPI) or overexpression of the lipase-inactive PLD2-K758R resulted in reduced nuclear localization of PLD independent of EGF stimulation. Following EGF stimulation, both the PABD sensor and PLD2-WT moved to cellular locations outside of the nucleus/perinucleus (Fig. 6A, lower panels).

This change in PA sensor localization was also evidenced as a change in the ratio of nuclear vs cytoplasmic staining of the PA sensor, which moved from Golgi/perinuclear to plasma membrane localization following EGF stimulation (Fig. 6B). Cooverexpression of both the PABD sensor and PLD2-WT resulted in colocalization in and around the nucleus in the absence of EGF (Fig. 6C). Collectively, these data suggest colocalization and trafficking of the PA sensor with PLD2 occurs in cells as a result of EGFR stimulation, which is dependent on catalytically active PLD2 and therefore the product of its reaction, PA.

3.6 PA Measurement in Tissues and After PLD Inhibitors: Lipid Extraction From Cells and Tissues

PA is a relatively minor cellular phospholipid. PA can be generated by sequential acylation of glycerol 3-phosphate which is a key step in the de novo synthesis of some glycerophospholipids and triglycerides (Athenstaedt & Daum, 1999). PA can also be formed by phosphorylation of diacylglycerol, and indeed PA and DG can be interconverted in cells through the actions of the relevant kinases and phosphatases (Merida, Avila-Flores, & Merino, 2008). As discussed elsewhere, PLD generates PA by hydrolysis of PC. PLD has the unique property of catalyzing transphosphatidylation reactions in which primary alcohols replace water as the nucleophile in the hydrolysis step of the PLD reaction. PLD-catalyzed transphosphatidylation generates phosphatidylalcohols which are not

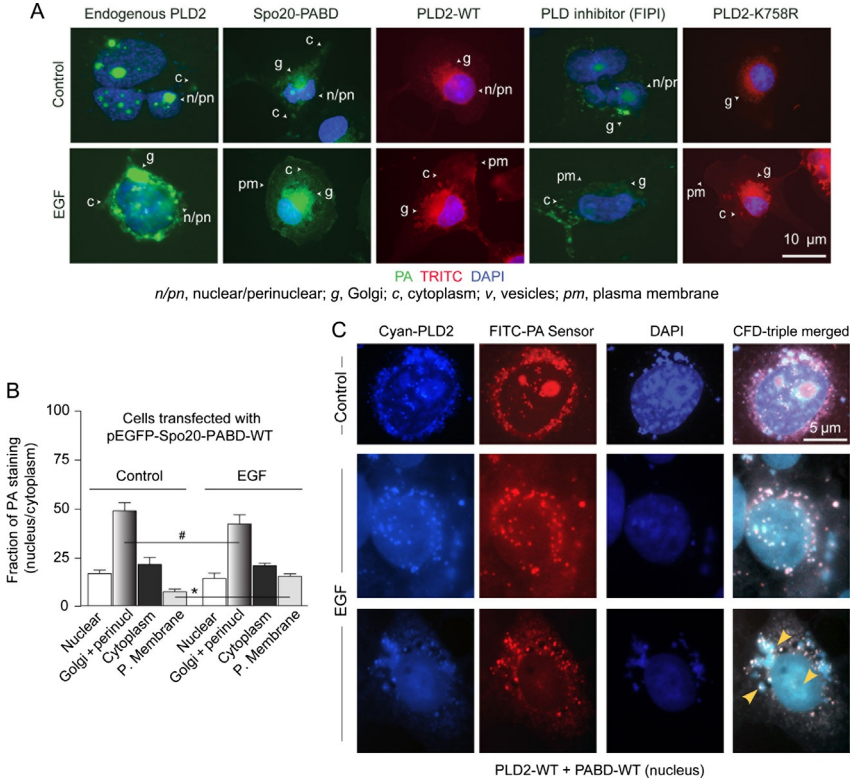

Fig. 6 PLD2 and PA colocalize to the nucleus. (A) COS-7 cells were fixed and then stained with α-PLD2-FITC antibodies to visualize endogenous PLD2 (in the absence or presence of the PLD-specific inhibitor FIPI), with α-PLD2-TRTC antibodies to visualize overexpressed PLD2 (-WT and -K758R) and/or with DAPI to visualize nuclei. The PA sensor was visualized using its GFP tag. Merged images of overlaid FITC and DAPI images or TRITC and DAPI images are shown. Abbreviations: *n/pn*, nuclear/perinuclear; *g*, Golgi; *c*, cytoplasm; *v*, vesicles; *pm*, plasma membrane. Scale bar = 10 μm. (B) Quantification of cellular immunofluorescence PA staining initially shifted from the Golgi and perinucleus (resting state) after 15 min incubation with 10 n*M* EGF to the plasma membrane using ImageJ software. The (*) *symbols* above *bars* denote statistically significant ($P < 0.05$) ANOVA increases between samples and controls. The (#) *symbols* above *bars* denote statistically significant ($P < 0.05$) ANOVA decreases between samples and controls. (C) Initial nuclear colocalization of both overexpressed PLD2-WT and overexpressed PA sensor in the absence of EGF is then colocalized away from the nucleus and out into the cytoplasm. Shown in this figure are images representative of $n = 3$ independent experiments with visualization of five similar fields in each condition. Scale bar = 5 μm.

naturally occurring in most cells and tissues and can be separated from other phospholipids by thin-layer chromatography (Liscovitch, Czarny, Fiucci, & Tang, 2000). Phosphatidylalcohols also appear to be more metabolically stable than PA, so their levels offer a robust way to report PLD activity in cells and tissues. However, the relative efficiency of the PLD-catalyzed hydrolysis and transphosphatidylation reactions in cells and tissues is difficult to determine and the relatively high concentrations of alcohols needed to achieve effective transphosphatidylation in cells and tissues are sufficiently high that nonspecific effects on cellular signaling and other biological processes remain a concern, as does the possibility that accumulation of phosphatidylalcohols has biological effects.

Accordingly, we have developed methods to directly measure changes in PA levels in cells and tissues that can be used to monitor PLD activity or test the efficacy of small-molecule PLD inhibitors (McDermott, Sigal, Crump, & Morris, 2006; Ren et al., 2010). These methods employ HPLC-coupled electrospray ionization tandem mass spectrometry on triple quadrupole instruments. Because PA is a family of lipids containing different fatty acids at the sn1 and sn2 groups of the glycerol moiety, these methods necessarily detect PA molecular species on the basis of the mass of their molecular ions, which is indicative of the total number of carbon atoms and degree of saturation of these fatty acid substituents. These methods can be modified to monitor fatty acid-derived anions generated by collisional dissociation of the molecular ion species. However, the methods described later monitor a common product ion species derived from the glycerol phosphate moiety which ionizes effectively ion negative ionization mode.

3.6.1 Material

- 8 mL Borosilicate glass tubes with Teflon cap
- PBS
- MeOH, $CHCl_3$, 0.1 *M* HCl
- C17 lysophosphatidic acid (LPA) (cat. # 857127), C-17 sphingosine 1-phosphate (S1P) (cat. # 860641) (both from Avanti Polar Lipids, Alabaster, AL, USA)

3.6.2 Protocol: Lipid Extraction From Cells and Tissues (Method Is Scaled for 35 mm Diameter Dishes/6-Well Plates)

1. Transfer cells to ice, remove culture medium, wash in ice-cold PBS, remove all liquid from cells.

2. Add 1 mL ice-cold MeOH to cells, scrape, transfer to borosilicate glass tube.
3. Add another 1 mL ice-cold MeOH to cells, scrape, transfer to same borosilicate glass tube.
4. Add 1 mL $CHCl_3$ and 0.5 mL 0.1 *M* HCl to tube.
5. Add internal standard (5–50 pmol C17 LPA, C-17 S1P as appropriate).
6. Vortex for 5 min (works best if you have a multitube vortexer).
7. Add 1 mL $CHCl_3$ and 1.3 mL 0.1 *M* HCl to separate phases.
8. Vortex for 5 min.
9. Centrifuge at $>3000 \times g$ for 10 min.
10. Transfer lower phase to 4 mL screw cap vial using a Pasteur pipette. Take care to avoid the protein interface and upper phase. Leave behind ~50 μL if needed (do not worry about being more accurate than this, as we have an internal standard to correct for recovery).
11. Evaporate to dryness under N_2 using N-evaporation in fume hood.
12. Resuspend in 1 mL 1:4 $CHCl_3$:MeOH.
13. If desired, remove 0.1–0.2 mL to a borosilicate 12×17 tube for phosphate determination.
14. Dry remaining sample under N_2, resuspend in 0.1 mL MeOH, vortex, and allow to air-dry for ~10 min.
15. Transfer to autosampler vial with glass or polypropylene insert for LC–MS analysis.

3.6.3 Protocol: Measurement of PA by HPLC ESI MS/MS

Extracted lipids are analyzed by reverse phase HPLC-coupled electrospray ionization tandem mass spectrometry. Studies reported from our laboratory have used ABSciex 4000 and 6500 series Q-Trap (hybrid triple quadrupole/linear ion trap) instruments operated in selected ion monitoring mode. These methods could be adapted to work with any gradient HPLC system coupled to a triple quadrupole mass spectrometer although in that case the instrument settings detailed later would have to be optimized for the selected system. The HPLC conditions and mass spectrometer settings used in our laboratory with an ABSciex 4000 Q-Trap system and a Shimadzu binary HPLC system are listed later.

LC conditions:

1. Column: Agilent Zorbax Eclipse XDB C8 column, 5 μm, 4.6×150 mm.
2. Solvent A: 75:25 = methanol/water, 0.5% formic acid + 0.1% ammonium formate.

Table 1 Gradient for LC Conditions

Time (min)	%B
0	0
2	0
3	100
11	100
12	100

3. Solvent B: 80 (99/1 = methanol/water, 0.5% formic acid + 0.1% ammonium formate): 20 (chloroform).
4. Flow rate: 0.5 mL/min; injection volume: 10 μL; oven temperature: 30°C; equilibration time: 3 min.
5. The gradient that should be used is shown in Table 1.

MS parameters (negative ESI):

1. Declustering potential (DP): −120.0 V; collision energy (CE): −56.0 V; collision cell exit potential (CXP): −13.0 V; CAD gas: medium; curtain gas: 20; ion spray voltage: −4500 V; temperature: 550.0°C; gas 1: 40.0 psi; gas 2: 40.0 psi.
2. The precursor and product ion masses monitored for the indicated PA species are shown in Table 2.

The data generated are integrated to determine chromatographic peak areas for the indicated ion pairs. In the method described earlier, we included C17 LPA as an internal standard hich was quantitated separately by HPLC MS/MS to calculate recovery of lipids throughout the procedure. The individual PA species were then quantitated by correcting integrated peak areas from the extracted ion chromatograms and use of external calibrations generated using authentic PA standards obtained from commercial sources that were independently quantitated by phosphorous determination after wet digestion in perchloric acid.

4. CONCLUSIONS AND OUTLOOK

Numerous biochemical approaches exist to discern PLD and PLD-mediated PA interactions with downstream signaling pathways in the cells, which we have defined herein to assist other researchers interested in phospholipases and phospholipid metabolism. Recent studies have focused on developing methods to directly measure changes in PA levels in cells and

Table 2 MS Parameters (Negative ESI) for Precursor and Product Ion Masses Monitored for the Indicated PA Species

		Q1 (Da)	Q3 (Da)	Time (ms)	DP (V)	CE (V)	CXP (V)
34-1	16:0–18:1(9z)	690.52	153	150	−120	−56	−13
43-6	21:0–22:6	806.58	153	150	−120	−56	−13
38-4	18:0–20:4	740.53	153	150	−120	−56	−13
34-1	16:0–18:1(11z)	673.49	153	150	−120	−56	−13
24-0	12:0–12:0	535.35	153	150	−120	−56	−13
28-0	14:0–14:0	591.41	153	150	−120	−56	−13
30-0	15:0–15:0	619.44	153	150	−120	−56	−13
32-0	16:0–16:0	647.47	153	150	−120	−56	−13
36-0	18:0–18:0	703.54	153	150	−120	−56	−13
36-4	18:2–18:2	695.47	153	150	−120	−56	−13
36-6	18:3–18:3	691.44	153	150	−120	−56	−13
32-1	14:0–18:1	645.46	153	150	−120	−56	−13
20-0	10:0–10:0	479.29	153	150	−120	−56	−13
34-0	16:0–18:2	671.47	153	150	−120	−56	−13
38-4	18:0–20:4	723.5	153	150	−120	−56	−1
36-4	16:0–20:4	699.5	153	150	−120	−56	−1
36-2	18:1–18:1	759.6	153	150	−120	−56	−1
40-0	18:0–22:0	701.52	153	150	−120	−56	−1
36-1	18:0–18:1	719.47	153	150	−120	−56	−1
38-6	16:0–22:6	747.5	153	150	−120	−56	−1
40-6	18:0–22:6	423.226	152.9	150	−95	−30	−7

tissues, which can be used to monitor PLD activity and even determine the effectiveness of small-molecule PLD inhibitors. Current and ongoing research interest in this field incorporating the use of PLD1 and PLD2-deficient mice and/or PLD-specific small-molecule inhibitors has identified possible roles for these two PLD isoforms in the development of cardiovascular disease and tumorigenesis, brain development, lipid metabolism, and leukocyte functions. PLD1 and PLD2 knockout mice are more prone to

be overweight, maintain a higher percent body fat, and develop diabetes as a function of age as a result of increased appetite and caloric intake compared to control mice (Trujillo Viera, El-Merahbi, Nieswandt, Stegner, & Sumara, 2016). Additionally, genetic and pharmacologic inhibition of PLD in mice results in protection against formation of stationary blood clots leading to improved stroke outcome (Elvers et al., 2010; Stegner et al., 2013). Tumor vascularization of melanoma or lung carcinoma was abolished in the tumor microenvironment of PLD1$^{-/-}$ mice (Chen et al., 2012), while use of PLD2-specific small-molecule inhibitors contributed to suppression of primary tumor growth and secondary metastases (Henkels, Boivin, Dudley, Berberich, & Gomez-Cambronero, 2013). Newborn mice lacking the two most common PLD isoforms suffer from diminished brain growth and astroglial proliferation, while adult mice deficient in PLD have impaired cognitive function, possibly due to significantly decreased brain acetylcholine levels (Burkhardt, Beyer, & Klein, 2015; Burkhardt et al., 2014). Lymphocytes from PLD1-deficient mice are less prone to adhere and migrate *in vitro* in mouse models of blood–brain barrier and cell migration (Gobel et al., 2014). Overall, future interest in PLD signaling research will undoubtedly focus on improving drug delivery and therapeutic effectiveness in many different models of human disease.

ACKNOWLEDGMENTS

Dr. Joel Swanson (University of Michigan School of Medicine) originally supplied the mCitrine plasmids used for subcloning of PLD2 and Rac2 for FRET analysis and also performed the FRET analyses. We would like to thank Denise Kramer for her help generating the PA sensor plasmids.

Funding: The following grants to Dr. Cambronero (J.G-C.) have supported this work: HL05665314 from the National Institutes of Health (NIH), 13GRNT17230097 from the American Heart Association (AHA), and 229102 20053 from the WSU Boonshoft School of Medicine (BSOM). Research in Dr. Morris's laboratory is supported by grants from the NIH, Department of Veterans Affairs, and Department of Defense.

REFERENCES

Athenstaedt, K., & Daum, G. (1999). Phosphatidic acid, a key intermediate in lipid metabolism. *European Journal of Biochemistry*, *266*, 1–16.

Bae, C. D., Min, D. S., Fleming, I. N., & Exton, J. H. (1998). Determination of interaction sites on the small G protein RhoA for phospholipase D. *The Journal of Biological Chemistry*, *273*, 11596–11604.

Best, R. B., Merchant, K. A., Gopich, I. V., Schuler, B., Bax, A., & Eaton, W. A. (2007). Effect of flexibility and cis residues in single-molecule FRET studies of polyproline. *Proceedings of the National Academy of Sciences of the United States of America*, *104*, 18964–18969.

Brandolini, L., Bertini, R., Bizzarri, C., Sergi, R., Caselli, G., Zhou, D., et al. (1996). IL-1 beta primes IL-8-activated human neutrophils for elastase release, phospholipase D activity, and calcium flux. *Journal of Leukocyte Biology*, *59*, 427–434.

Burkhardt, U., Beyer, S., & Klein, J. (2015). Role of phospholipases D1 and 2 in astroglial proliferation: Effects of specific inhibitors and genetic deletion. *European Journal of Pharmacology*, *761*, 398–404.

Burkhardt, U., Stegner, D., Hattingen, E., Beyer, S., Nieswandt, B., & Klein, J. (2014). Impaired brain development and reduced cognitive function in phospholipase D-deficient mice. *Neuroscience Letters*, *572*, 48–52.

Chae, Y. C., Kim, K. L., Ha, S. H., Kim, J., Suh, P. G., & Ryu, S. H. (2010). Protein kinase Cdelta-mediated phosphorylation of phospholipase D controls integrin-mediated cell spreading. *Molecular and Cellular Biology*, *30*, 5086–5098.

Chen, Q., Hongu, T., Sato, T., Zhang, Y., Ali, W., Cavallo, J. A., et al. (2012). Key roles for the lipid signaling enzyme phospholipase d1 in the tumor microenvironment during tumor angiogenesis and metastasis. *Science Signaling*, *5*, ra79.

Chen, Y., Muller, J. D., Ruan, Q., & Gratton, E. (2002). Molecular brightness characterization of EGFP in vivo by fluorescence fluctuation spectroscopy. *Biophysical Journal*, *82*, 133–144.

Colley, W. C., Sung, T. C., Roll, R., Jenco, J., Hammond, S. M., Altshuller, Y., et al. (1997). Phospholipase D2, a distinct phospholipase D isoform with novel regulatory properties that provokes cytoskeletal reorganization. *Current Biology*, 7, 191–201.

Cummings, R. J., Parinandi, N. L., Zaiman, A., Wang, L., Usatyuk, P. V., Garcia, J. G., et al. (2002). Phospholipase D activation by sphingosine 1-phosphate regulates interleukin-8 secretion in human bronchial epithelial cells. *The Journal of Biological Chemistry*, *277*, 30227–30235.

Elvers, M., Stegner, D., Hagedorn, I., Kleinschnitz, C., Braun, A., Kuijpers, M. E., et al. (2010). Impaired alpha(IIb)beta(3) integrin activation and shear-dependent thrombus formation in mice lacking phospholipase D1. *Science Signaling*, *3*, ra1.

Faugaret, D., Chouinard, F. C., Harbour, D., El azreq, M. A., & Bourgoin, S. G. (2010). An essential role for phospholipase D in the recruitment of vesicle amine transport protein-1 to membranes in human neutrophils. *Biochemical Pharmacology*, *81*, 144–156.

Gambin, Y., & Deniz, A. A. (2010). Multicolor single-molecule FRET to explore protein folding and binding. *Molecular BioSystems*, *6*, 1540–1547.

Gobel, K., Schuhmann, M. K., Pankratz, S., Stegner, D., Herrmann, A. M., Braun, A., et al. (2014). Phospholipase D1 mediates lymphocyte adhesion and migration in experimental autoimmune encephalomyelitis. *European Journal of Immunology*, *44*, 2295–2305.

Gomez-Cambronero, J. (2014). Phosphatidic acid, phospholipase D and tumorigenesis. *Advances in Biological Regulation*, *54*, 197–206.

Gurskaya, N. G., Fradkov, A. F., Pounkova, N. I., Staroverov, D. B., Bulina, M. E., Yanushevich, Y. G., et al. (2003). A colourless green fluorescent protein homologue from the non-fluorescent hydromedusa Aequorea coerulescens and its fluorescent mutants. *The Biochemical Journal*, *373*, 403–408.

Hammond, S. M., Altshuller, Y. M., Sung, T. C., Rudge, S. A., Rose, K., Engebrecht, J., et al. (1995). Human ADP-ribosylation factor-activated phosphatidylcholine-specific phospholipase D defines a new and highly conserved gene family. *The Journal of Biological Chemistry*, *270*, 29640–29643.

Hammond, S. M., Jenco, J. M., Nakashima, S., Cadwallader, K., Gu, Q., Cook, S., et al. (1997). Characterization of two alternately spliced forms of phospholipase D1. Activation of the purified enzymes by phosphatidylinositol 4,5-bisphosphate, ADP-ribosylation factor, and Rho family monomeric GTP-binding proteins and protein kinase C-alpha. *The Journal of Biological Chemistry*, *272*, 3860–3868.

Hanahan, D. J., & Chaikoff, I. L. (1947a). A new phospholipide-splitting enzyme specific for the ester linkage between the nitrogenous base and the phosphoric acid grouping. *The Journal of Biological Chemistry*, *169*, 699–705.

Hanahan, D. J., & Chaikoff, I. L. (1947b). The phosphorous-containing lipids of the carrot. *The Journal of Biological Chemistry*, *168*, 233–240.

Hatton, N., Lintz, E., Mahankali, M., Henkels, K. M., & Gomez-Cambronero, J. (2015). Phosphatidic acid increases epidermal growth factor receptor expression by stabilizing mRNA decay and by inhibiting lysosomal and proteasomal degradation of the internalized receptor. *Molecular and Cellular Biology*, *35*, 3131–3144.

Henkels, K. M., Boivin, G. P., Dudley, E. S., Berberich, S. J., & Gomez-Cambronero, J. (2013). Phospholipase D (PLD) drives cell invasion, tumor growth and metastasis in a human breast cancer xenograph model. *Oncogene*, *32*, 5551–5562.

Henkels, K. M., Mahankali, M., & Gomez-Cambronero, J. (2013). Increased cell growth due to a new lipase-GEF (Phospholipase D2) fastly acting on Ras. *Cellular Signalling*, *25*, 198–205.

Henkels, K. M., Mallets, E. R., Dennis, P. B., & Gomez-Cambronero, J. (2015). S6K is a morphogenic protein with a mechanism involving Filamin-A phosphorylation and phosphatidic acid binding. *FASEB Journal*, *29*, 1299–1313.

Hermansson, M., Hokynar, K., & Somerharju, P. (2011). Mechanisms of glycerophospholipid homeostasis in mammalian cells. *Progress in Lipid Research*, *50*, 240–257.

Hoppe, A., Christensen, K., & Swanson, J. A. (2002). Fluorescence resonance energy transfer-based stoichiometry in living cells. *Biophysical Journal*, *83*, 3652–3664.

Iqbal, A., Arslan, S., Okumus, B., Wilson, T. J., Giraud, G., Norman, D. G., et al. (2008). Orientation dependence in fluorescent energy transfer between Cy3 and Cy5 terminally attached to double-stranded nucleic acids. *Proceedings of the National Academy of Sciences of the United States of America*, *105*, 11176–11181.

Jain, R. K., Joyce, P. B., Molinete, M., Halban, P. A., & Gorr, S. U. (2001). Oligomerization of green fluorescent protein in the secretory pathway of endocrine cells. *The Biochemical Journal*, *360*, 645–649.

Jang, J. H., Lee, C. S., Hwang, D., & Ryu, S. H. (2012). Understanding of the roles of phospholipase D and phosphatidic acid through their binding partners. *Progress in Lipid Research*, *51*, 71–81.

Jeon, H., Kwak, D., Noh, J., Lee, M. N., Lee, C. S., Suh, P. G., et al. (2011). Phospholipase D2 induces stress fiber formation through mediating nucleotide exchange for RhoA. *Cellular Signalling*, *23*, 1320–1326.

Kim, J. H., Lee, S. D., Han, J. M., Lee, T. G., Kim, Y., Park, J. B., et al. (1998). Activation of phospholipase D1 by direct interaction with ADP-ribosylation factor 1 and RalA. *FEBS Letters*, *430*, 231–235.

Kodaki, T., & Yamashita, S. (1997). Cloning, expression, and characterization of a novel phospholipase D complementary DNA from rat brain. *The Journal of Biological Chemistry*, *272*, 11408–11413.

Kong, H. J., Polte, T. R., Alsberg, E., & Mooney, D. J. (2005). FRET measurements of cell-traction forces and nano-scale clustering of adhesion ligands varied by substrate stiffness. *Proceedings of the National Academy of Sciences of the United States of America*, *102*, 4300–4305.

Lee, C. S., Kim, J. M., Ghim, J., Suh, P. G., & Ryu, S. H. (2015). GTP-dependent interaction between phospholipase D and dynamin modulates fibronectin-induced cell spreading. *Cellular Signalling*, *27*, 2363–2370.

Lee, C. S., Kim, I. S., Park, J. B., Lee, M. N., Lee, H. Y., Suh, P. G., et al. (2006). The phox homology domain of phospholipase D activates dynamin GTPase activity and accelerates EGFR endocytosis. *Nature Cell Biology*, *8*, 477–484.

Lee, J. G., Lee, S. H., Park, D. W., Bae, Y. S., Yun, S. S., Kim, J. R., et al. (2007). Phosphatidic acid as a regulator of matrix metalloproteinase-9 expression via the TNF-alpha signaling pathway. *FEBS Letters*, *581*, 787–793.

Lehman, N., Di Fulvio, M., McCray, N., Campos, I., Tabatabaian, F., & Gomez-Cambronero, J. (2006). Phagocyte cell migration is mediated by phospholipases PLD1 and PLD2. *Blood*, *108*, 3564–3572.

Liscovitch, M., Czarny, M., Fiucci, G., & Tang, X. (2000). Phospholipase D: Molecular and cell biology of a novel gene family. *The Biochemical Journal*, *345*(Pt. 3), 401–415.

Mahankali, M., Farkaly, T., Bedi, S., Hostetler, H. A., & Gomez-Cambronero, J. (2015). Phosphatidic acid (PA) can displace PPARalpha/LXRalpha binding to the EGFR promoter causing its transrepression in luminal cancer cells. *Scientific Reports*, *5*, 15379.

Mahankali, M., Henkels, K. M., Alter, G., & Gomez-Cambronero, J. (2012). Identification of the catalytic site of phospholipase D2 (PLD2) newly described guanine nucleotide exchange factor activity. *The Journal of Biological Chemistry*, *287*, 41417–41431.

Mahankali, M., Henkels, K. M., & Gomez-Cambronero, J. (2013). A GEF-to-phospholipase molecular switch caused by phosphatidic acid, Rac and JAK tyrosine kinase that explains leukocyte cell migration. *Journal of Cell Science*, *126*, 1416–1428.

Mahankali, M., Henkels, K. M., Speranza, F., & Gomez-Cambronero, J. (2015). A non-mitotic role for Aurora kinase A as a direct activator of cell migration upon interaction with PLD, FAK and Src. *Journal of Cell Science*, *128*, 516–526.

Mahankali, M., Peng, H. J., Henkels, K. M., Dinauer, M. C., & Gomez-Cambronero, J. (2011). Phospholipase D2 (PLD2) is a guanine nucleotide exchange factor (GEF) for the GTPase Rac2. *Proceedings of the National Academy of Sciences of the United States of America*, *108*, 19617–19622.

Matz, M. V., Fradkov, A. F., Labas, Y. A., Savitsky, A. P., Zaraisky, A. G., Markelov, M. L., et al. (1999). Fluorescent proteins from nonbioluminescent Anthozoa species. *Nature Biotechnology*, *17*, 969–973.

McDermott, M. I., Sigal, Y. J., Crump, J. S., & Morris, A. J. (2006). Enzymatic analysis of lipid phosphate phosphatases. *Methods*, *39*, 169–179.

Merida, I., Avila-Flores, A., & Merino, E. (2008). Diacylglycerol kinases: At the hub of cell signalling. *The Biochemical Journal*, *409*, 1–18.

Nakanishi, H., de los Santos, P., & Neiman, A. M. (2004). Positive and negative regulation of a SNARE protein by control of intracellular localization. *Molecular Biology of the Cell*, *15*, 1802–1815.

Pathre, P., Shome, K., Blumental-Perry, A., Bielli, A., Haney, C. J., Alber, S., et al. (2003). Activation of phospholipase D by the small GTPase Sar1p is required to support COPII assembly and ER export. *The EMBO Journal*, *22*, 4059–4069.

Peng, H. J., Henkels, K. M., Mahankali, M., Dinauer, M. C., & Gomez-Cambronero, J. (2011a). Evidence for two CRIB domains in phospholipase D2 (PLD2) that the enzyme uses to specifically bind to the small GTPase Rac2. *The Journal of Biological Chemistry*, *286*, 16308–16320.

Peng, H. J., Henkels, K. M., Mahankali, M., Marchal, C., Bubulya, P., Dinauer, M. C., et al. (2011b). The dual effect of Rac2 on phospholipase D2 regulation that explains both the onset and termination of chemotaxis. *Molecular and Cellular Biology*, *31*, 2227–2240.

Powner, D. J., & Wakelam, M. J. (2002). The regulation of phospholipase D by inositol phospholipids and small GTPases. *FEBS Letters*, *531*, 62–64.

Ren, H., Federico, L., Huang, H., Sunkara, M., Drennan, T., Frohman, M. A., et al. (2010). A phosphatidic acid binding/nuclear localization motif determines lipin1 function in lipid metabolism and adipogenesis. *Molecular Biology of the Cell*, *21*, 3171–3181.

Rose, K., Rudge, S. A., Frohman, M. A., Morris, A. J., & Engebrecht, J. (1995). Phospholipase D signaling is essential for meiosis. *Proceedings of the National Academy of Sciences of the United States of America*, *92*, 12151–12155.

Saito, M., & Kanfer, J. (1973). Solubilization and properties of a membrane-bound enzyme from rat brain catalyzing a base-exchange reaction. *Biochemical and Biophysical Research Communications*, *53*, 391–398.

Sanematsu, F., Nishikimi, A., Watanabe, M., Hongu, T., Tanaka, Y., Kanaho, Y., et al. (2013). Phosphatidic acid-dependent recruitment and function of the Rac activator DOCK1 during dorsal ruffle formation. *The Journal of Biological Chemistry*, *288*, 8092–8100.

Speranza, F. J., Mahankali, M., & Gomez-Cambronero, J. (2013). Macrophage migration arrest due to a winning balance of Rac2/Sp1 repression over beta-catenin-induced PLD expression. *Journal of Leukocyte Biology*, *94*, 953–962.

Speranza, F., Mahankali, M., Henkels, K. M., & Gomez-Cambronero, J. (2014). The molecular basis of leukocyte adhesion involving phosphatidic acid and phospholipase D. *The Journal of Biological Chemistry*, *289*, 28885–28897.

Stace, C. L., & Ktistakis, N. T. (2006). Phosphatidic acid- and phosphatidylserine-binding proteins. *Biochimica et Biophysica Acta*, *1761*, 913–926.

Stegner, D., Thielmann, I., Kraft, P., Frohman, M. A., Stoll, G., & Nieswandt, B. (2013). Pharmacological inhibition of phospholipase D protects mice from occlusive thrombus formation and ischemic stroke—Brief report. *Arteriosclerosis, Thrombosis, and Vascular Biology*, *33*, 2212–2217.

Trujillo Viera, J., El-Merahbi, R., Nieswandt, B., Stegner, D., & Sumara, G. (2016). Phospholipases D1 and D2 suppress appetite and protect against overweight. *PLoS One*, *11*, e0157607.

VanBeek, D. B., Zwier, M. C., Shorb, J. M., & Krueger, B. P. (2007). Fretting about FRET: Correlation between kappa and R. *Biophysical Journal*, *92*, 4168–4178.

Wang, X., Dyer, J. H., & Zheng, L. (1993). Purification and immunological analysis of phospholipase D from castor bean endosperm. *Archives of Biochemistry and Biophysics*, *306*, 486–494.

Wang, X., Xu, L., & Zheng, L. (1994). Cloning and expression of phosphatidylcholine-hydrolyzing phospholipase D from Ricinus communis L. *The Journal of Biological Chemistry*, *269*, 20312–20317.

Yamazaki, M., Zhang, Y., Watanabe, H., Yokozeki, T., Ohno, S., Kaibuchi, K., et al. (1999). Interaction of the small G protein RhoA with the C terminus of human phospholipase D1. *The Journal of Biological Chemistry*, *274*, 6035–6038.

Zeniou-Meyer, M., Zabari, N., Ashery, U., Chasserot-Golaz, S., Haeberle, A. M., Demais, V., et al. (2007). Phospholipase D1 production of phosphatidic acid at the plasma membrane promotes exocytosis of large dense-core granules at a late stage. *The Journal of Biological Chemistry*, *282*, 21746–21757.

Zhang, F., Wang, Z., Lu, M., Yonekubo, Y., Liang, X., Zhang, Y., et al. (2014). Temporal production of the signaling lipid phosphatidic acid by phospholipase D2 determines the output of extracellular signal-regulated kinase signaling in cancer cells. *Molecular and Cellular Biology*, *34*, 84–95.